

## Supporting Information

### Selective electrooxidation of 5-hydroxymethylfurfural to 5-formyl-furan-2-formic acid on non-metallic polyaniline catalysts: Structure-function relationships

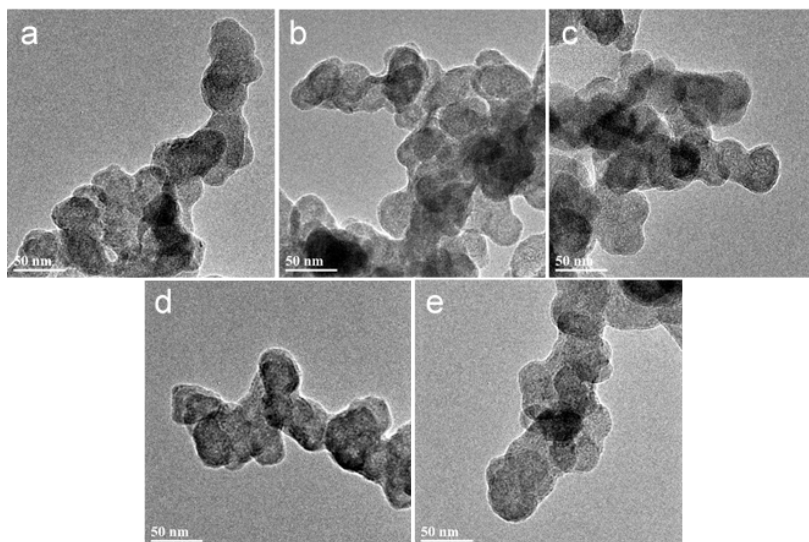
Xingyu Lu<sup>a,b</sup>, Ke Qi<sup>a,b</sup>, Xueya Dai<sup>a,b</sup>, Yunlong Li<sup>a,b</sup>, Di Wang<sup>c</sup>, Jing Dou<sup>a,b</sup>, Wei Qi<sup>a,b\*</sup>

<sup>a</sup> Shenyang National Laboratory for Materials Science Institute of Metal Research, Chinese Academy of Sciences Shenyang, Liaoning, China

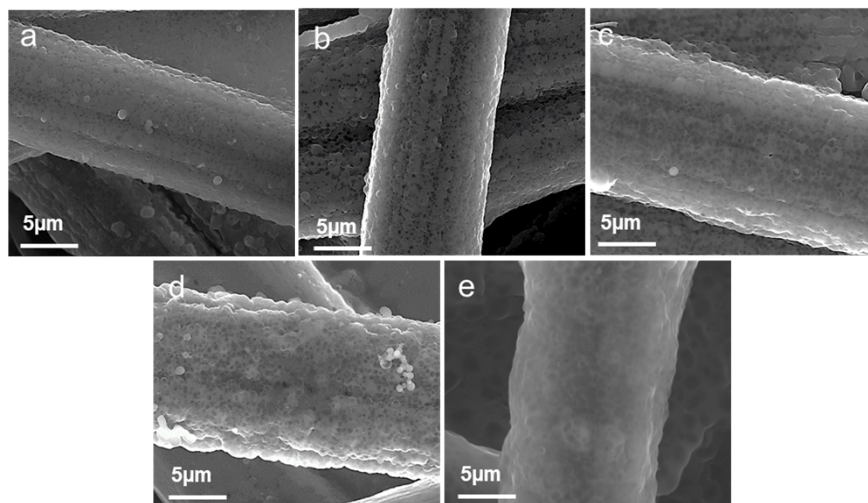
<sup>b</sup> School of Materials Science and Engineering University of Science and Technology of China Shenyang, Liaoning, China

<sup>c</sup> School of Pharmacy, Shenyang Pharmaceutical University, No.26 Huatuo Rd, High & New Tech Development Zone, Benxi, Liaoning Province, China.

\*Email: wqi@imr.ac.cn



**Fig. S1.** TEM images of (a) PANI<sub>2</sub>/CP, (b) PANI<sub>3</sub>/CP, (c) PANI<sub>4</sub>/CP, (d) PANI<sub>5</sub>/CP and (e) PANI<sub>6</sub>/CP catalysts.



**Fig. S2.** SEM images of (a) PANI<sub>2</sub>/CP, (b) PANI<sub>3</sub>/CP, (c) PANI<sub>4</sub>/CP, (d) PANI<sub>5</sub>/CP and (e) PANI<sub>6</sub>/CP catalysts.

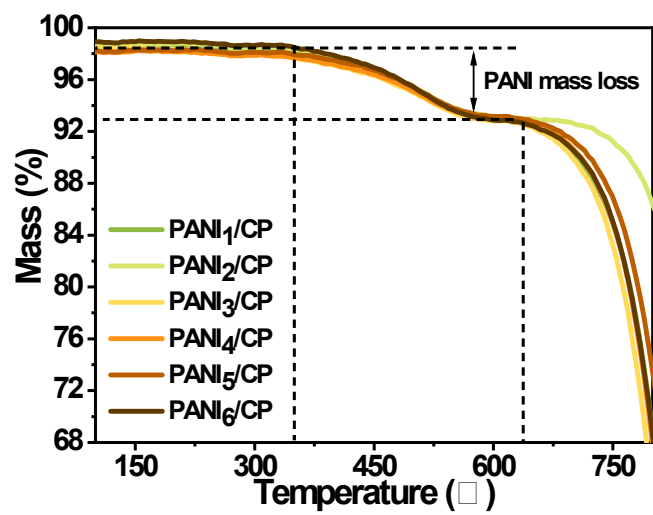
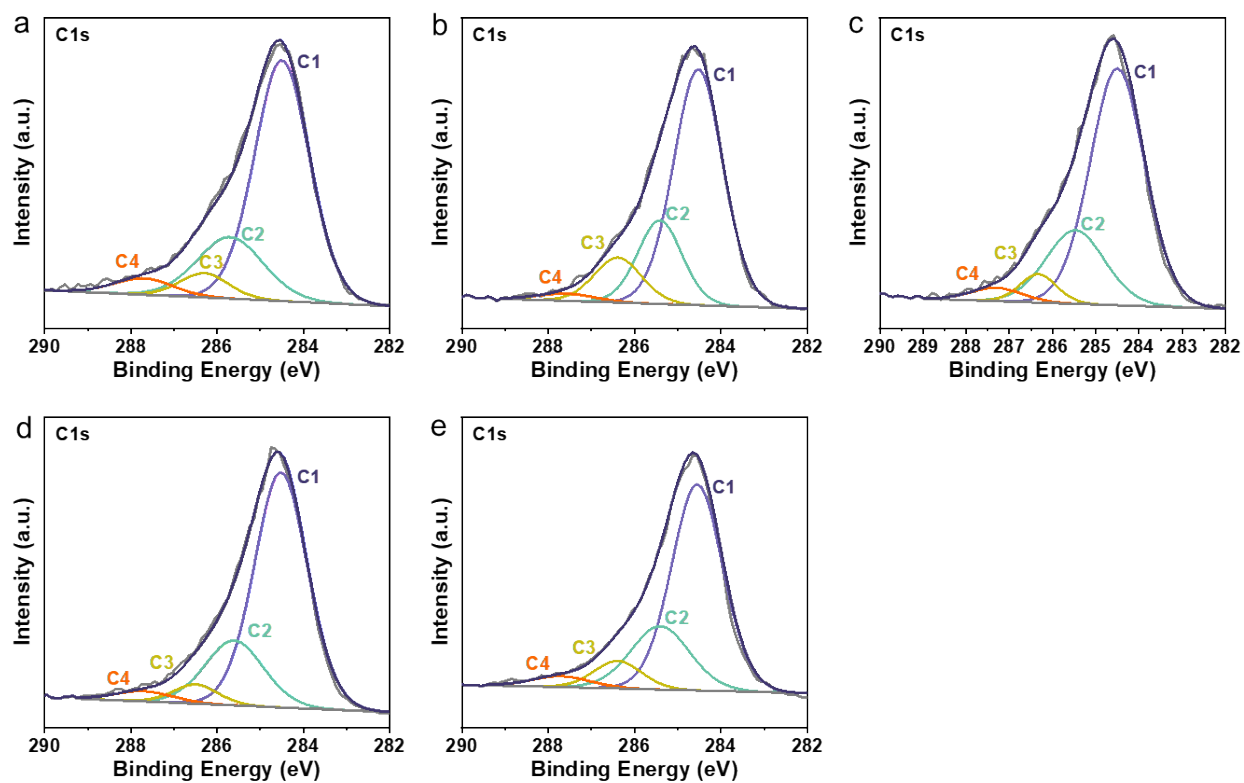
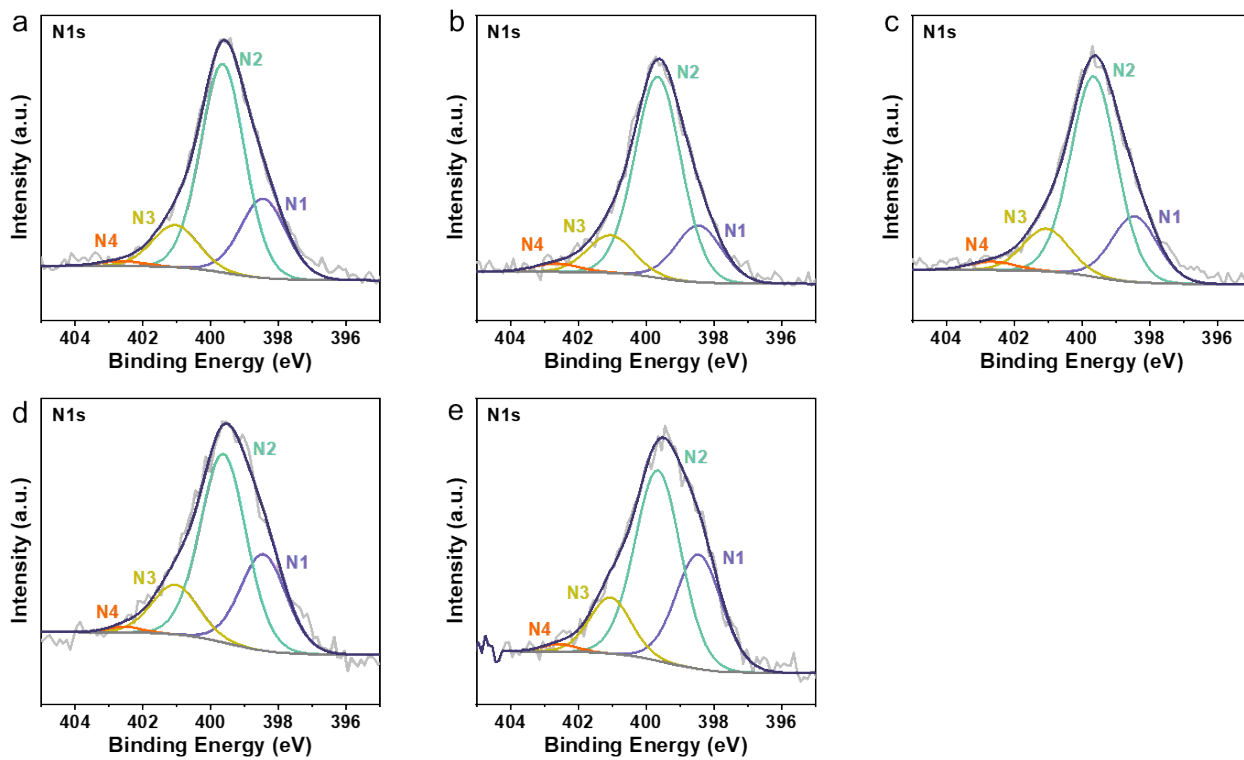


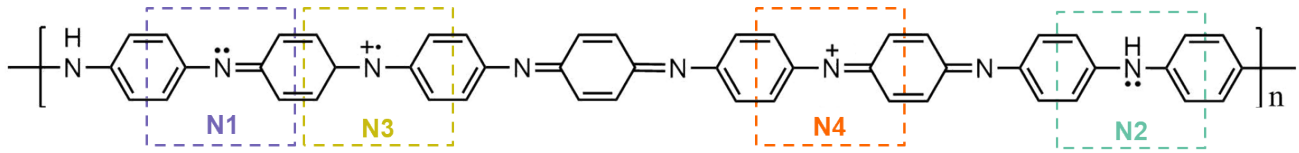
Fig. S3. TGA profiles of all PANI/CP catalysts in air.



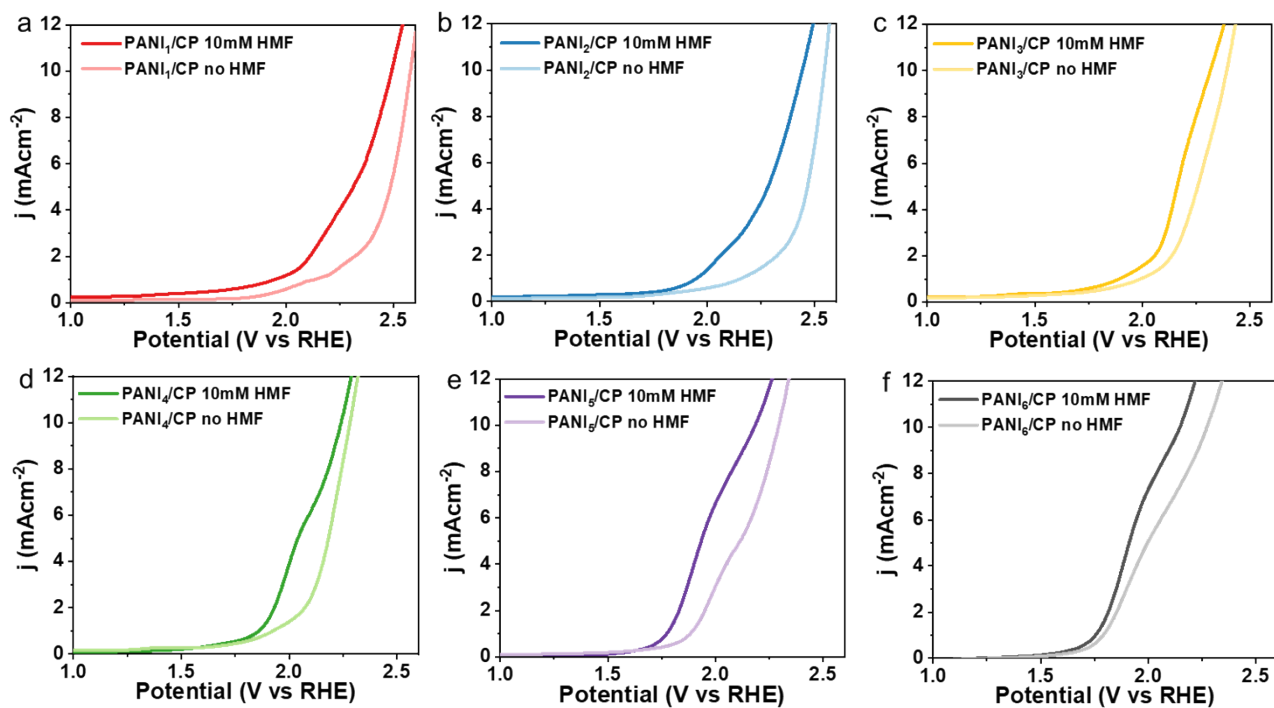
**Fig. S4.** Deconvoluted C 1s XPS spectra of a) PANI<sub>2</sub>/CP, b) PANI<sub>3</sub>/CP, c) PANI<sub>4</sub>/CP, d) PANI<sub>5</sub>/CP and e) PANI<sub>6</sub>/CP catalysts.



**Fig. S5.** Deconvoluted N1s XPS spectra of a) PANI<sub>2</sub>/CP, b) PANI<sub>3</sub>/CP, c) PANI<sub>4</sub>/CP, d) PANI<sub>5</sub>/CP and e) PANI<sub>6</sub>/CP catalysts.

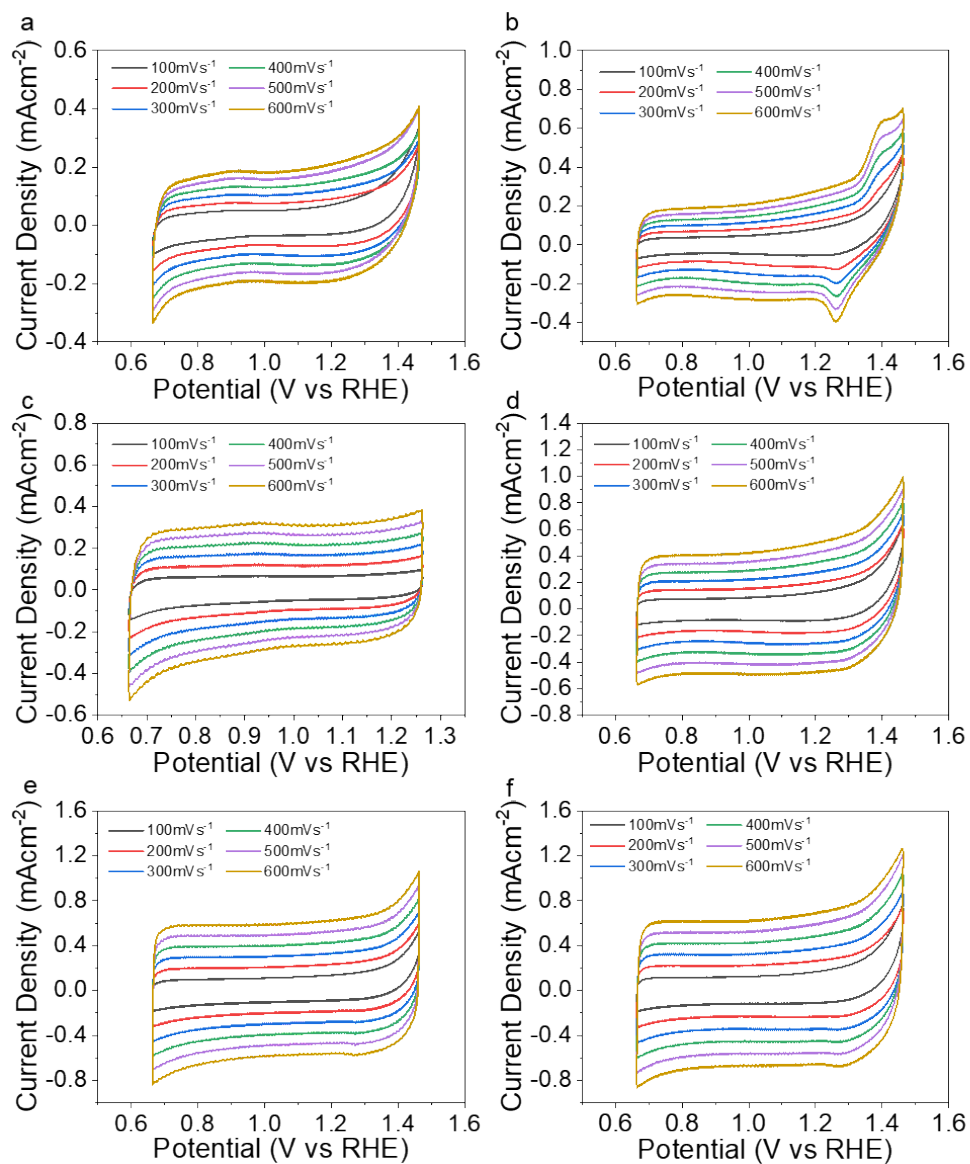


**Fig. S6.** Chemical structure diagram of polyaniline.

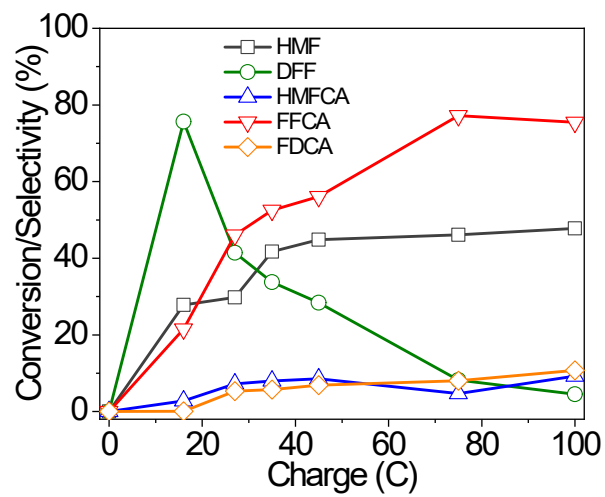


**Fig. S7.** Linear sweep voltammetry curves of a) PANI<sub>1</sub>/CP, b) PANI<sub>2</sub>/CP, c) PANI<sub>3</sub>/CP, d) PANI<sub>4</sub>/CP, e) PANI<sub>5</sub>/CP and f) PANI<sub>6</sub>/CP samples with 10 mM HMF or without HMF in 0.1 M KOH solution (pH 13) at the scan rate of 10 mV s<sup>-1</sup>.

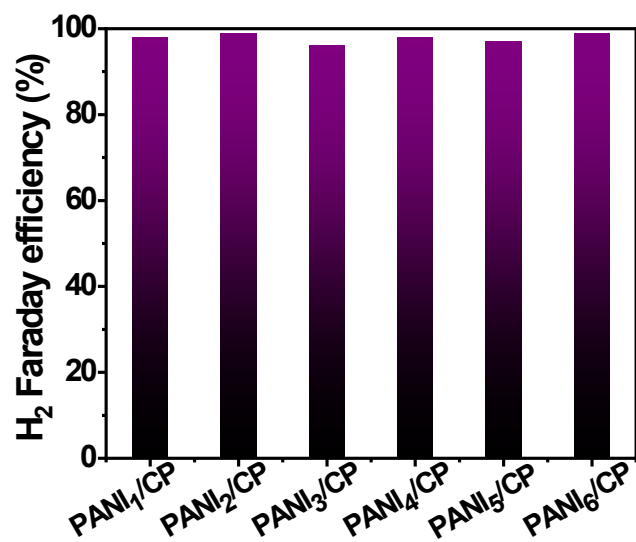




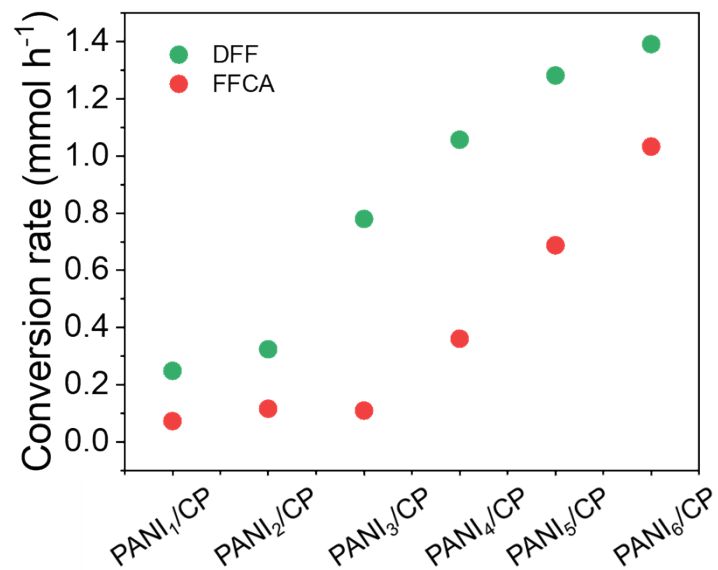
**Fig. S8.** CV curves of a) PANI<sub>1</sub>/CP, b) PANI<sub>2</sub>/CP, c) PANI<sub>3</sub>/CP, d) PANI<sub>4</sub>/CP, e) PANI<sub>5</sub>/CP and f) PANI<sub>6</sub>/CP samples at different scan rate from 100 mV s<sup>-1</sup> to 600 mV s<sup>-1</sup> in 0.1 M KOH solution with 10 mM HMF.



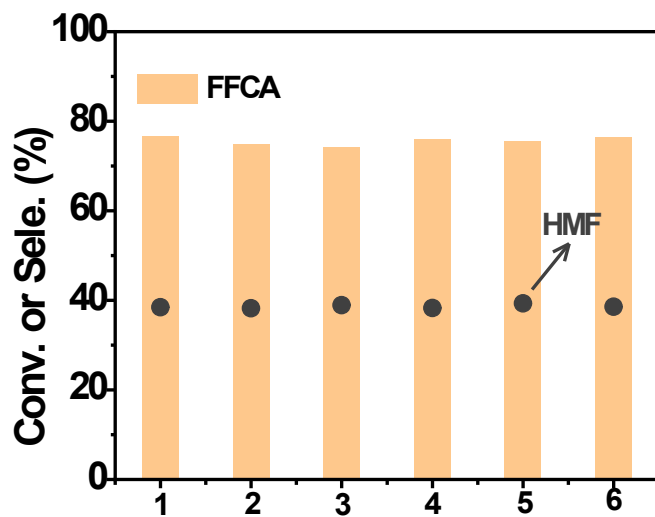
**Fig. S9.** Conversion of HMF and selectivity of its oxidation products with PANI<sub>4</sub>/CP electrode catalyst as function of charge at potential of 1.96 V<sub>RHE</sub>.



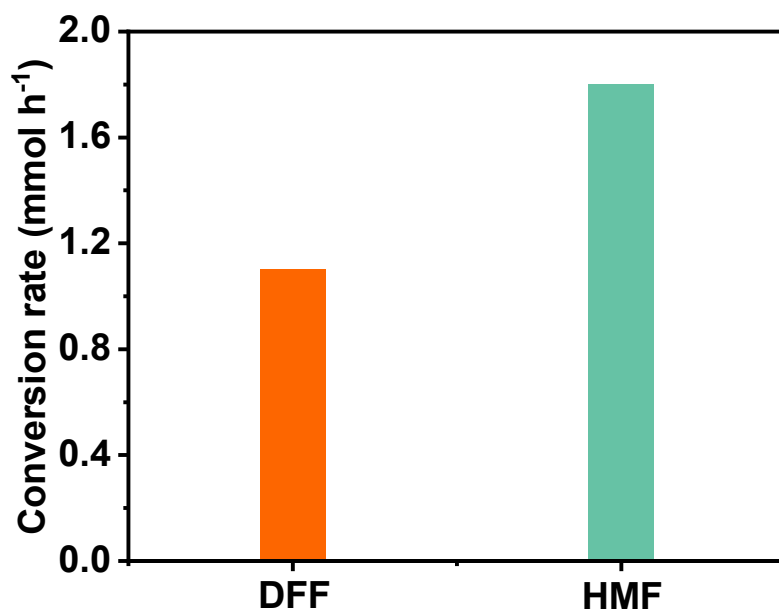
**Fig. S10.** H<sub>2</sub> Faradaic efficiency on Pt cathode for all PANI/CP catalysts.



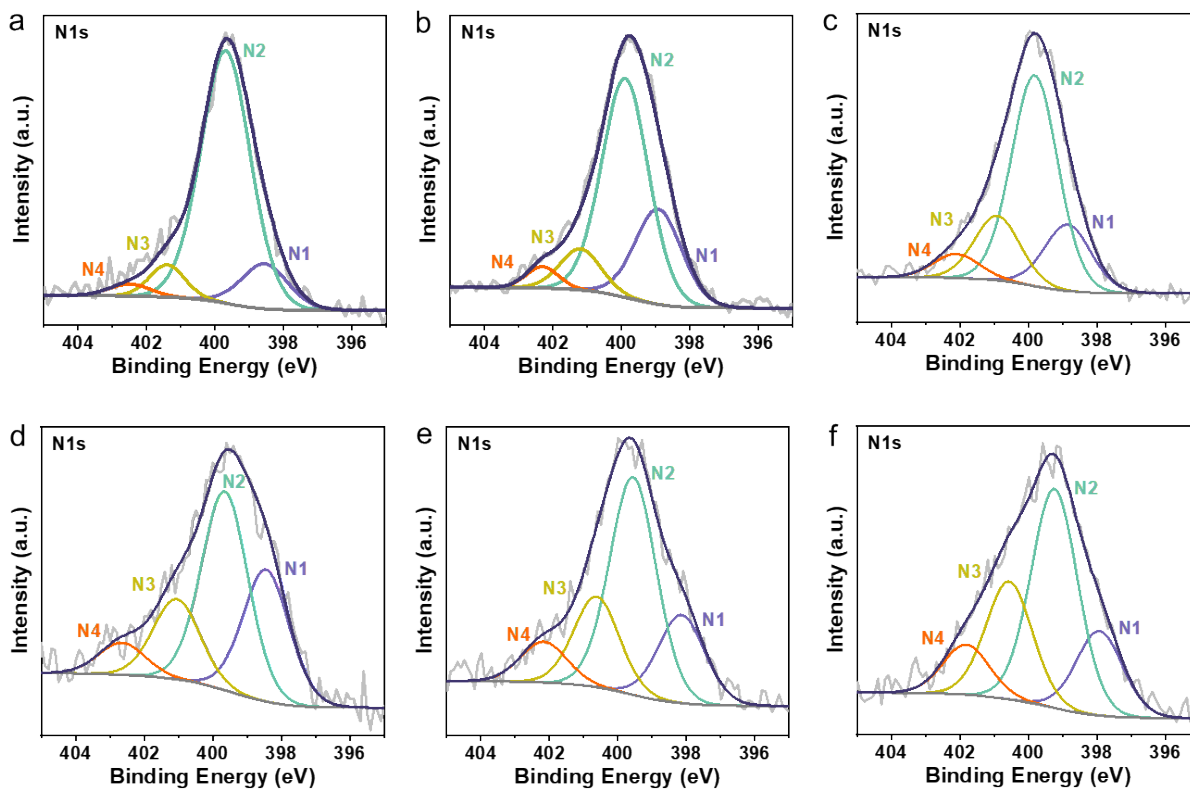
**Fig. S11.** Conversion rates of DFF or FFCA for all PANI/CP samples when DFF or FFCA as the reactant until transferred 28.8 C electrons at potential of 1.96 V<sub>RHE</sub>.



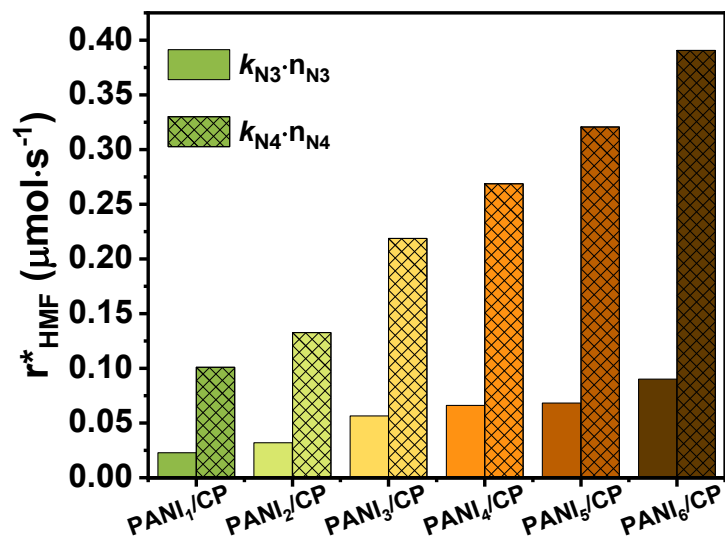
**Fig. S12.** Conversion of HMF, selectivity of FFCA of PANI<sub>4</sub>/CP sample at potential of 1.96 V<sub>RHE</sub> after 6 cycles.



**Fig. S13.** Conversion rates of HMF or DFF for PANI<sub>4</sub>/CP sample when HMF or DFF as the reactant, respectively at potential of 1.96 V<sub>RHE</sub>.

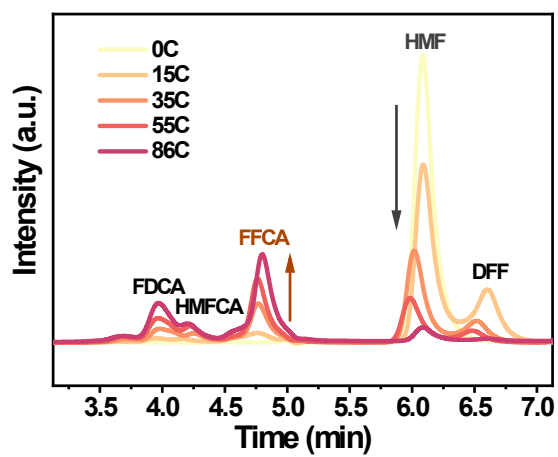


**Fig. S14.** Deconvoluted N1s XPS spectra of a) PANI<sub>1</sub>/CP, b) PANI<sub>2</sub>/CP, c) PANI<sub>3</sub>/CP, d) PANI<sub>4</sub>/CP, d) PANI<sub>5</sub>/CP and e) PANI<sub>6</sub>/CP samples after HMFOR reaction.

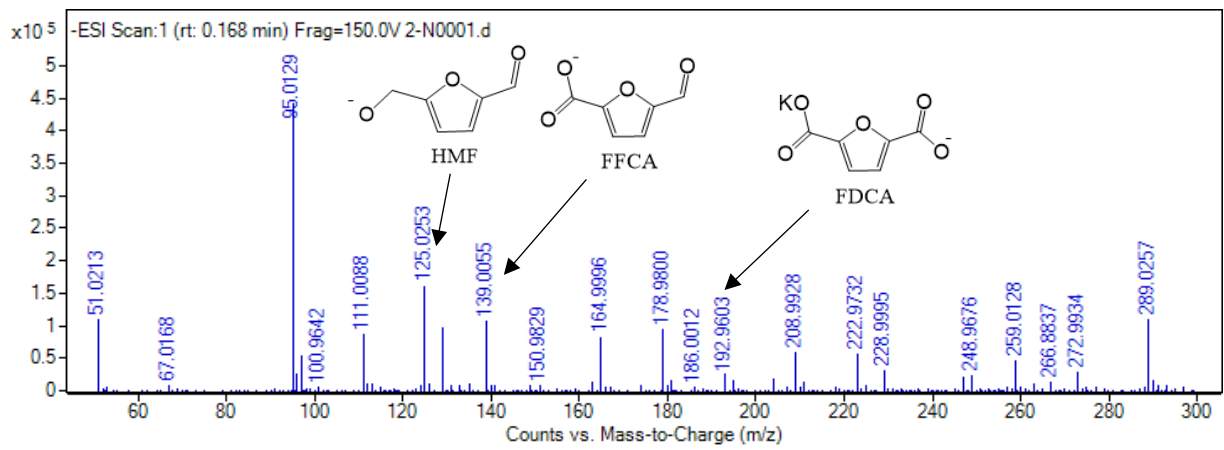


**Fig. S15.** Contribution of N4 and N3 to HMFOR after considering the number of active sites in catalysts, where  $r^*_{\text{HMF}}$  is the theoretical conversion rate of HMF.

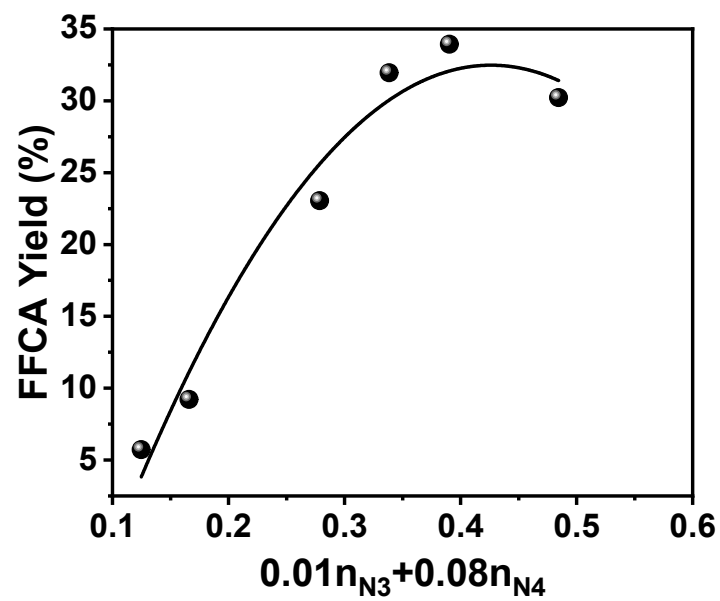




**Fig. S16.** High performance liquid chromatography analysis results for all reactants and products during the HMF electrooxidation reaction for PANI<sub>4</sub>/CP catalyst.


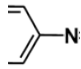

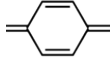


**Fig. S17.** Mass spectrometry spectra of the electrolyte after the reaction with PANI<sub>4</sub>/CP catalyst.

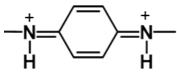
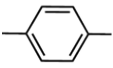
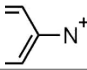
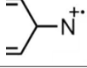
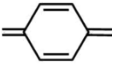


**Fig. S18.** Contribution of all active sites (oxidation capacity) of PANI catalysts as a function of yield of FFCA.

**Table S1.** Assignments of FT-IR peak of all PANI/CP catalysts.

Peak position (cm <sup>-1</sup> )	Assignments	Structure
1154	N=Q=N absorption peaks (Q represents the quinoid ring)	
1307	C-N stretching mode	
1495	C=C stretching vibration of the benzenoid rings	
1585	C=C stretching vibration of the quinoid rings	

**Table S2.** Assignments of Raman bands of all PANI/CP catalysts at an excitation of 532 nm.

peak position ( $\text{cm}^{-1}$ )	Assignments	Structure
412	Out of plane C-H wag in polaronic structures	
606	Benzenoid ring in plane deformation	
1255	C-N stretching in polaronic units	
1376	C-N <sup>+</sup> stretching of radical cations	
1560	C-C stretching of quinoid rings	

**Table S3.** HMFOR performance of PANI/CP and catalysts.

Entry	Catalyst	Electrolyte/HMF concentration	pH	Catalyst loading (mg cm <sup>-2</sup> )	Potential (V <sub>RHE</sub> )	HMF Conv.	Product/Sele.
1	PANI/CP	0.1 M KOH/10 mM	13	1	1.96	43%	FFCA/76%
2	NiO/CP	0.1 M KOH/10 mM	13	1	1.36	98%	FDCA/100%
3	CuO/CP	0.1 M KOH/10 mM	13	1	1.46	96%	FDCA/100%
4	Polypyrrole/CP	0.1 M KOH/10 mM	13	1	1.96	18%	DFF/60%
5	Polythiophene/CP	0.1 M KOH/10 mM	13	1	1.96	12%	DFF/54%

**Table S4.** HMFOR performance of PANI/CP and other reported catalysts.

Entry	Catalyst	Electrolyte/HMF concentration	pH	Catalyst loading (mg cm <sup>-2</sup> )	Potential (V <sub>RHE</sub> )	HMF Conv.	Product/Sele.	Ref.
1	PANI/CP	0.1 M KOH/10 mM	13	1	1.96	43%	FFCA/76%	This work
2	NC	0.1 M NaOH/5 mM	13	0.3	1.90	15%	FDCA/26% <sup>a</sup>	1
	BNC					71%	FDCA/80% <sup>a</sup>	
3	Ru-NiO	1.0 M PBS/50 mM	6.9	NA	1.50	55%	DFF/61% <sup>a</sup>	2
4	Ni(NS)	0.1 M KOH/5 mM	13	NA	1.36	99.7%	FDCA/99.7%	3
5	CoO-CoSe <sub>2</sub>	1.0 M KOH/10 mM	14	5	1.43	100%	FDCA/96%	4
6	CuCo <sub>2</sub> O <sub>4</sub>	1.0 M KOH/50 mM	14	0.2	1.45	98%	FDCA/95.6% <sup>a</sup>	5
7	Ir-Co <sub>3</sub> O <sub>4</sub>	1.0 M KOH/50 mM	12	NA	1.42	≥99% <sup>a</sup>	FDCA/98% <sup>a</sup>	6
8	Ni <sub>3</sub> S <sub>2</sub>	1.0 M KOH/10 mM	14	NA	1.423	≥99% <sup>a</sup>	FDCA/97% <sup>a</sup>	7
9	MoO <sub>2</sub> -FeP@C	1.0 M KOH/10 mM	14	1.9	1.424	99.4%	FDCA/98%	8
10	(FeCrCoNiCu) <sub>3</sub> O <sub>4</sub>	1.0 M KOH/50 mM	14	0.8	1.50	≥99% <sup>a</sup>	FDCA/97% <sup>a</sup>	9
11	N-Co <sub>3</sub> O <sub>4</sub>	1.0 M KOH/50 mM	14	NA	1.423	99.5%	FDCA/97.8%	10
12	PdAu/C	0.1 M KOH/50 mM	13	NA	0.90	≥99% <sup>a</sup>	FDCA/83% <sup>a</sup>	11
13	Pt/Ni(OH) <sub>2</sub>	1.0 M KOH/50 mM	14	0.2	NA	≥99% <sup>a</sup>	FDCA96% <sup>a</sup>	12

<sup>a</sup> Data that is not listed explicitly in the literature. NA: not available.

**Table S5.** Contents of N1, N2, N3 and N4 groups on the PANI/CP catalysts after HMFOR reaction from N1s.

Material	N1 %	N2 %	N3 %	N4 %	N1 $\mu\text{mol}$	N2 $\mu\text{mol}$	N3 $\mu\text{mol}$	N4 $\mu\text{mol}$	$r_{\text{HMF}} \mu\text{mol}\cdot\text{s}^{-1}$
PANI <sub>1</sub> /CP	12.89	77.16	6.95	3.01	5.18	27.84	2.80	1.21	0.08
PANI <sub>2</sub> /CP	26.09	59.95	9.90	4.06	9.97	21.46	3.89	1.59	0.15
PANI <sub>3</sub> /CP	18.30	57.70	17.39	6.61	7.27	22.91	6.90	2.62	0.28
PANI <sub>4</sub> /CP	29.77	44.83	18.17	7.24	13.23	19.92	8.08	3.22	0.30
PANI <sub>5</sub> /CP	20.26	49.98	20.37	9.39	8.29	20.44	8.33	3.84	0.38
PANI <sub>6</sub> /CP	17.92	46.46	25.00	10.62	7.89	20.45	11.01	4.68	0.46



**Note S1.** The contents of N1, N2, N3 and N4 groups on the PANI/CP catalysts are calculated from XPS results. The Equation (1), (2), (3) and (4) are as following:

$$N1 (mmol) = \frac{N\% \times N1\% \times 6 \text{ mg}}{12 \times C\% + 16 \times O\% + 14 \times N\%}$$

(1)

$$N2 (mmol) = \frac{N\% \times N2\% \times 6 \text{ mg}}{12 \times C\% + 16 \times O\% + 14 \times N\%}$$

(2)

$$N3 (mmol) = \frac{N\% \times N3\% \times 6 \text{ mg}}{12 \times C\% + 16 \times O\% + 14 \times N\%}$$

(3)

$$N4 (mmol) = \frac{N\% \times N4\% \times 6 \text{ mg}}{12 \times C\% + 16 \times O\% + 14 \times N\%}$$

(4)

**Note S2.** Identification and quantification of active sites for HMFOR via the conversion rate of HMF transformation (the fitting process).

The experimental observed the conversion rate of HMF transformation ( $r_{HMF}$ ) as dependent variables are linearly fitted with concentration of N3 and N4 functional groups as independent variables using  $k$  as fitting parameters.  $k$  represents the number of HMF reactant converted per mole of active site per second. The derived Equation (5) is as following:

$$r_{HMF} = k_{N3} \cdot n_{N3} + k_{N4} \cdot n_{N4} \quad (5)$$

Where  $r_{HMF}$ ,  $n_{N3}$  and  $n_{N4}$  represent the conversion rate of HMF transformation and concentration of N3 and N4 on catalysts, respectively.

## Reference<sup>1-15</sup>

1. Qin, Q. et al. Electrochemical fixation of nitrogen and its coupling with biomass valorization with a strongly adsorbing and defect optimized boron–carbon–nitrogen catalyst. *ACS Appl. Energy Mater.*, **2**, 8359-8365, (2019).
2. Ge, R. et al. Selective electrooxidation of biomass-derived alcohols to aldehydes in a neutral medium: Promoted water dissociation over a nickel-oxide-supported ruthenium single-atom catalyst. *Angew. Chem. Int. Ed.*, **61**, e202200211, (2022).
3. Lu, X. et al. Highly efficient electro-reforming of 5-hydroxymethylfurfural on vertically oriented nickel nanosheet/carbon hybrid catalysts: Structure-function relationships. *Angew. Chem. Int. Ed.*, **60**, 14528-14535, (2021).
4. Huang, X. et al. Enhancing the electrocatalytic activity of CoO for the oxidation of 5-hydroxymethylfurfural by introducing oxygen vacancies. *Green Chem.*, **22**, 843-849, (2020).
5. Lu, Y. et al. Identifying the Geometric Site Dependence of Spinel Oxides for the Electrooxidation of 5-Hydroxymethylfurfural. *Angew. Chem. Int. Ed.*, **59**, 19215-19221, (2020).
6. Lu, Y. X. et al. Tuning the Selective Adsorption Site of Biomass on Co<sub>3</sub>O<sub>4</sub> by Ir Single Atoms for Electrosynthesis. *Adv. Mater.*, **33**, 6, (2021).
7. You, B. Liu, X. Jiang, N. & Sun, Y. A General Strategy for Decoupled Hydrogen Production from Water Splitting by Integrating Oxidative Biomass Valorization. *J. Am. Chem. Soc.*, **138**, 13639-13646, (2016).
8. Yang, G. et al. Interfacial Engineering of MoO<sub>2</sub>-FeP Heterojunction for Highly Efficient Hydrogen Evolution Coupled with Biomass Electrooxidation. *Adv. Mater.*, **32**, e2000455, (2020).
9. Gu, K. et al. Defect-Rich High-Entropy Oxide Nanosheets for Efficient 5-Hydroxymethylfurfural Electrooxidation. *Angew. Chem. Int. Ed.*, **60**, 20253-20258, (2021).
10. Sun, M. et al. Nitrogen-doped Co<sub>3</sub>O<sub>4</sub> nanowires enable high-efficiency electrochemical oxidation of 5-hydroxymethylfurfural. *Chinese Chemical Letters*, **33**, 385-389, (2022).
11. Chadderdon, D. J. et al. Electrocatalytic oxidation of 5-hydroxymethylfurfural to 2,5-furandicarboxylic acid on supported Au and Pd bimetallic nanoparticles. *Green Chem.*, **16**, 3778-3786, (2014).
12. Zhou, B. et al. Platinum modulates redox properties and 5-hydroxymethylfurfural adsorption kinetics of Ni(OH)<sub>2</sub> for biomass upgrading. *Angew. Chem. Int. Ed.*, **60**, 22908-22914, (2021).